

Revealing Structure and Crystallographic Orientation of Soft Epitaxial Assembly of Nanocrystals by Grazing Incidence X-ray Scattering

Santanu Maiti,^{*,†,#} Alexander André,[‡] Sonam Maiti,^{†,‡} Martin Hodas,[†] Maciej Jankowski,[§] Marcus Scheele,^{‡,||} and Frank Schreiber^{†,||}

[†]Institute of Applied Physics, University of Tübingen, Auf der Morgenstelle 10, 72076 Tübingen, Germany

[#]Jülich Centre of Neutron Science (JCNS-1), Forschungszentrum Jülich GmbH, 52425 Jülich, Germany

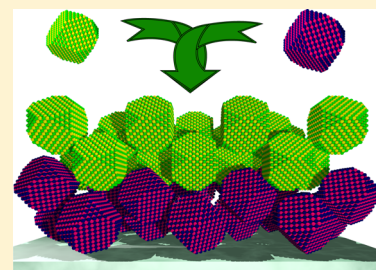
[‡]Institute of Physical and Theoretical Chemistry, University of Tübingen, Auf der Morgenstelle 18, 72076 Tübingen, Germany

[§]ID03, ESRF - The European Synchrotron, 71 Avenue des Martyrs, F-38000 Grenoble, France

^{||}Center for Light-Matter Interaction, Sensors & Analytics LISA+, University of Tübingen, Auf der Morgenstelle 15, 72076 Tübingen, Germany

S Supporting Information

ABSTRACT: We study the structural coherence of a self-assembled overlayer of PbS nanocrystal (NC) superlattice onto an underlying PbS NC monolayer, which acts as a template. We explore the effect of the templating layer on the structure of the overlayer assemblies by varying interfacial strain and determine the impact of new ligands on their superlattice structure. The overlayers and templates are analyzed by grazing-incidence X-ray scattering and microscopy. We find that differences in the lattice parameters of 7.7% between the two layers are tolerated in terms of a “soft epitaxial” assembly into the body-centered tetragonal superstructure and lead to structural registry within the overlayer. Conversely, at the interface, a lattice mismatch of 24.4% is too large for soft epitaxy and invokes a change in the superlattice. Upon ligand treatment, the overlayer superlattices transform their orientation axis and the NCs orient preferentially. These results provide new insights into mitigating defects in layered, heterostructured NC assemblies.



Atomic and molecular epitaxy has been extensively used in semiconductor technology to fabricate near-perfect interfaces of adlayers on top of a crystalline substrate. In such systems, the atoms or molecules are the basic building blocks of the structure and the substrate acts as a guiding template.^{1–3} In conventional semiconductor technology, control over the interface between two stacks in a multilayered device (e.g., a p–n junction) is one of the most crucial steps in the fabrication process, with a large impact on the overall device performance.^{4–7} Stacked multilayers of self-assembled semiconductor NCs and control over their structure along in- and out-of-plane directions are of high importance for many device applications, for instance (light-emitting) diodes or photovoltaic modules.^{8–17} Defect-free epitaxial growth of the next layer onto a first layer acting as a template is an important precondition for efficient carrier separation and transport across the interface. This ability is likely to be equally important in stacked NC devices; however, means to achieve a similar degree of control remain largely unexplored to date.^{18–23}

In the past, only a few initiatives have been employed to grow epitaxial assemblies of NCs, and their focus was mainly on characterization at the microscopic level using electron microscopy. In most cases, extreme experimental conditions (e.g., annealing of the superlattice assembly at elevated

temperatures, complex interfaces, or lithographically defined pattern substrates) have been used to organize them.^{24–29} Moreover, these synthesis methods often lead to adverse atomically connected NCs, where the individual building blocks lost their own identity^{19–21} and often lack the ability to produce long-range coherent superstructures of NCs with desired superlattice orientation. Therefore, it is very crucial to determine not only the structure and orientation of the epitaxial assembly but also the atomic alignment of the NCs within the superstructure with respect to the template. Recently, a superlattice consisting of alternating NCs and organic semiconductor (OSC) molecules has been proposed, where NCs assemble via a coordinating OSC through preferential binding to their facets, commonly known as coupled organic–inorganic nanostructures (COINs).^{30–33} Using these COINs as the guiding template, a comprehensive approach has been employed to prepare an epitaxially grown NC assembly at ambient conditions.

In this work, we prepare “hexagonal” and “square” periodic COIN templates by single-layer PbS NCs cross-linked with

Received: August 14, 2019

Accepted: September 20, 2019

Published: September 20, 2019

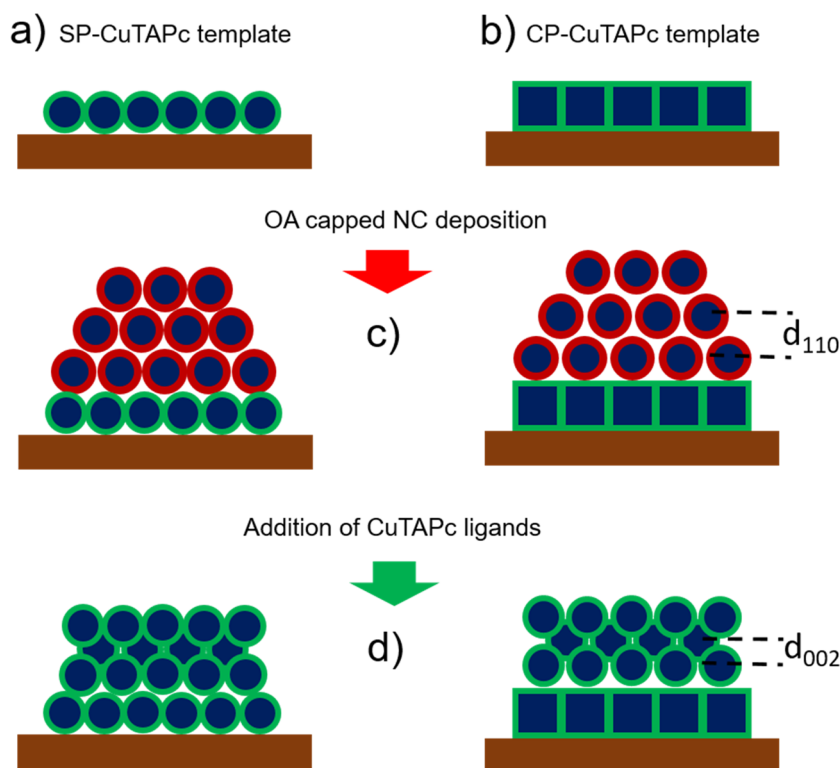


Figure 1. Scheme of the NC assemblies. (a) Hexagonally ordered SP-CuTAPc template and (b) square periodic CP-CuTAPc template. (c) Deposition of NC adlayers on the surface of designed templates. (d) CuTAPc ligand-induced assemblies of NCs.

copper β -tetraaminophthalocyanine (CuTAPc) molecules and deposit colloidal PbS NCs on the top surface of the templates under ambient conditions. The adlayer NC assemblies are then treated with CuTAPc ligands at room temperature. The template monolayers and the adlayer assemblies are systematically characterized by grazing incidence small-angle X-ray scattering (GISAXS), scanning electron microscopy (SEM), and atomic force microscopy (AFM). The structure, symmetry, and orientation of the superlattices are obtained by X-ray scattering within the framework of the distorted wave Born approximation^{34–36} (DWBA) and explained on the basis of lattice misfit and lattice reconstruction. Furthermore, the atomic-ordering of the NCs within the superlattices is determined by grazing incidence X-ray diffraction (GIXD).

Here, we use two different types of PbS NCs: spherical (diameter ~ 8.0 nm) and faceted cubic (length ~ 11.8 nm) (Figure S1), abbreviated as spherical particle or “SP” and cubic particle or “CP”, respectively. We symbolize the atomic properties of nanocrystals and superlattice properties of the superstructure with the subscripts “NC” and “SL”, respectively. Figure 1 describes a schematic of the superlattices at different stages (details of the preparation procedures are provided in the Supporting Information), and they are abbreviated in Table 1. We first fabricate ordered COIN templates of SP and CP NCs coupled with CuTAPc (Figure 1a,b). The second step

is the deposition of NCs on the surface of the designed templates (Figure 1c). Ligand treatment with CuTAPc molecules on the deposited NCs is the last step of the sample preparation (Figure 1d).

Characterization of Templates. While details are provided as Supporting Information (Figure S2), in brief, we characterize the SP-CuTAPc COINs template by GISAXS, GIXD, XRR, and microscopy to compare with the structure of the overlayer assemblies. The results indicate the SP NCs order into a 2D hexagonally ordered superlattice monolayer with a lattice parameter of 9.7 ± 0.1 nm. We also prepare square periodic superlattices of a PbS NC monolayer (CP-CuTAPc template) with a lattice parameter of 12.8 ± 0.1 nm, and their detailed characterization was performed on another occasion.³⁰

Overlayer of SP NCs on a SP-CuTAPc Template. The GISAXS pattern for the deposited spherical NC assembly (SP@OA) on the surface of the SP-CuTAPc template is shown in Figure 2a. The presence of several scattering peaks corresponds to an ordered superstructure formation on top of the hexagonal template. The scattering peaks are indexed to a body-centered tetragonal (bct) superlattice (SG: $Im\bar{3}m$) of $a = b = 10.7$ nm and $c = 9.27$ nm, oriented with the $[110]_{SL}$ axis perpendicular to the template. The GISAXS pattern obtained for the ligand-induced assembly looks very different (Figure 2b) from the as-deposited NC adlayers, which implies the formation of well-ordered superlattices of different types. The scattering peaks are simulated and indexed to a body-centered cubic (bcc) superlattice (SG: $Im\bar{3}m$) of $a = b = c = 10.4$ nm, oriented with the $[002]_{SL}$ axis normal to the template (Table S1). The axial orientational transformation of the superlattice is confirmed by real space SEM images (Figure S3). In the GIXD profiles and patterns of the corresponding adlayer assemblies, we observe the most intense diffraction peaks from $\{111\}_{NC}$ planes and

Table 1. Sample Specifications

COINs template	deposited adlayer NCs (@)	ligand-induced adlayer (+)
hexagonal SP-CuTAPc	SP@OA	SP + CuTAPc
square CP-CuTAPc	SP@OA	SP + CuTAPc

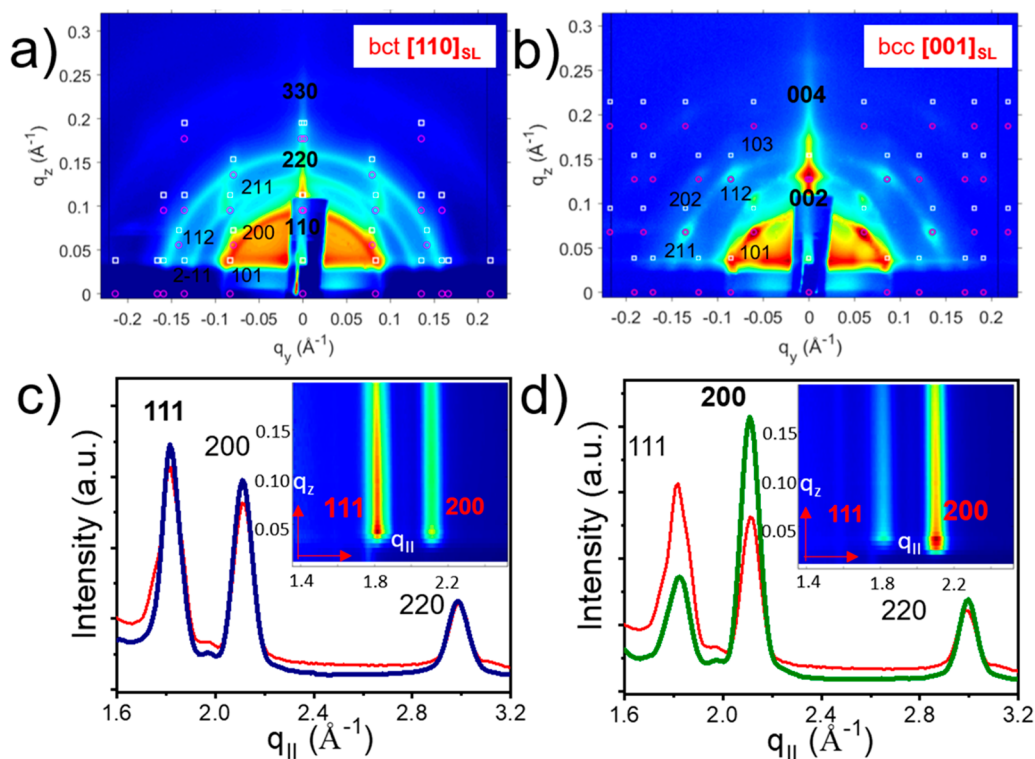


Figure 2. GISAXS patterns of the (a) deposited SP@OA and (b) ligand-induced assembly. The pink circles (transmitted) and white boxes (reflected) denote the simulated diffraction peaks. GIXD profiles as a function of $q_{||}$ from the (c) SP@OA and (d) ligand-induced assembly along with the profile of SP-CuTAPc template (red lines) for comparison. Insets: corresponding 2D GIXD patterns in q -space.

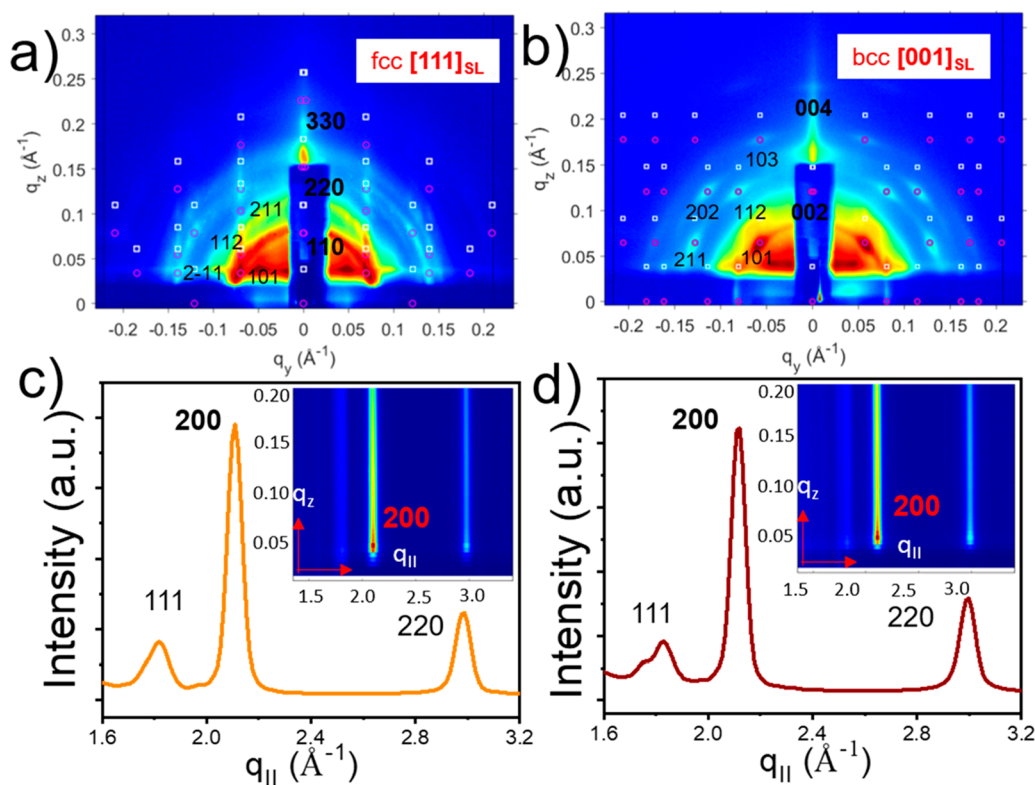


Figure 3. GISAXS patterns of the (a) drop-casted SP NCs (SP@OA) and (b) ligand-induced assembly. The pink circles (transmitted) and white boxes (reflected) denote the simulated diffraction peaks. GIXD line profiles as a function of $q_{||}$ from the (c) SP@OA and (d) ligand-induced assembly. Insets: corresponding 2D GIXD patterns in q -space.

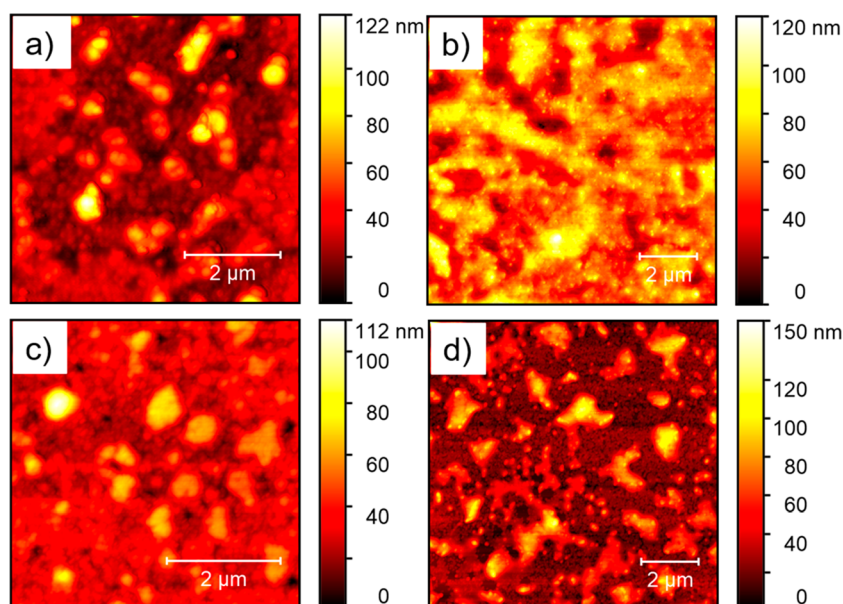


Figure 4. AFM images of (a) deposited SP@OA and (b) ligand-treated assemblies on top of the SP-CuTAPc template. AFM images of (c) deposited SP@OA and (d) ligand-treated assemblies on top of the CP-CuTAPc template.

relatively less intense scattering from $\{200\}_{\text{NC}}$ planes (Figure 2c), whereas their ligand-induced counterpart has a sharp and directional scattering from the $\{200\}_{\text{NC}}$ planes (Figure 2d). These types of diffraction patterns are also evident in the GIWAXS patterns (Figure S4), collected along the out-of-plane direction.

Overlayer of SP NCs on a CP-CuTAPc Template. Panels a and b of Figure 3 shows the GISAXS patterns for the deposited spherical NC assembly (SP@OA) and the corresponding CuTAPc-induced NC assembly on the surface of the CP-CuTAPc template, respectively. For both cases, we observe many well-defined scattering peaks but different patterns, which illustrate that the NCs organize into ordered assemblies of an altered lattice structure. The GISAXS pattern for the drop-casted NC assembly is indexed according to a face-centered cubic (fcc) superlattice (SG: $Fm\bar{3}m$) of $a = 14.7$ nm, oriented with the $[111]_{\text{SL}}$ axis normal to the template (Table S2). In contrast, the GISAXS pattern for the ligand-induced assembly is indexed to a bcc superlattice (SG: $Im\bar{3}m$) of $a = 11.0$ nm, oriented with the $[002]_{\text{SL}}$ axis perpendicular to the template. These results are corroborated with SEM images of the adlayer superlattices in Figure S5. GIXD profiles and patterns for both of the assemblies (Figure 3c,d, inset) have a strong and directional diffraction peak from the $\{200\}_{\text{NC}}$ planes as provided by the 200_{NC} Bragg reflection.

Growth of NCs on the Templates. The AFM images for the as-deposited NC assemblies on the hexagonally ordered SP-CuTAPc template (Figure 4a) and square periodic CP-CuTAPc template (Figure 4c) show typical “plateau-like” soft epitaxial islands with smooth tops, having in-plane domain size of 200–500 nm and height of 60–80 nm (Figure S6). Here, the overall growth mechanism is very similar to the Volmer–Weber (VW) growth mode where the objects grow into discrete islands on top of the substrate. The AFM images of the ligand-induced NC assemblies (Figure 4b,d) on the surface of either square or hexagonally ordered templates show a different film morphology in the entire film, which is probably due to the structural modification in the assembly via

adligands. These structural changes are already demonstrated by the transformed scattering patterns and real space images.

The growth of soft epitaxial nanostructures is discussed based on the identification of the growth mode and determination of their complex structure. As the epitaxial assemblies essentially depend on the lattice parameters of the template and adlayers, here we initiated the lattice misfit by varying the size and shapes of NCs and their surface ligands. The lattice misfit is defined as $f = (y - x)/x$, where “ x ” and “ y ” are the center-to-center distance of the NCs in the templates and adlayer lattices, respectively. The effective size of the NCs and the misfits are provided in Tables 2 and 3.

Table 2. Size Misfit of NCs Compared to the SP-CuTAPc Template

sample	core diameter (nm)	ligand size (nm)	effective diameter (nm)	lattice mismatch (%) f_1
SP-CuTAPc template	8.0	1.0 ± 0.4	9.0	NA
SP@OA adlayer	8.0	1.8 ± 0.5	9.8	+7.7
ligand-induced SP	8.0	1.0 ± 0.4	9.0	0 (−7.7)

We observe that the as-deposited PbS NCs (SP, 8.0 nm) self-assemble into two different superlattices with varied lattice

Table 3. Size Misfit of NCs Compared to the CP-CuTAPc Template

sample	core diameter (nm)	ligand size (nm)	effective diameter (nm)	lattice mismatch (%) f_2
CP-CuTAPc template	11.8	1.0 ± 0.4	12.8	NA
SP@OA adlayer	8.0	1.8 ± 0.5	9.8	−24.4
ligand-induced SP	8.0	1.0 ± 0.4	9.0	−29 (−7)

parameters on top of two differently designed NC templates (see Figures 2 and 3 and Tables 2 and 3). If the interfacial mismatch = 7.7%, we observe the formation of a bct superlattice and that it has an in-plane lattice parameter of $a = b = 10.7$ nm and contracted $c = 9.27$ nm; whereas if the mismatch = -24.4%, then the NCs self-assemble into an fcc superlattice with a lattice parameter of $a = b = c = 14.7$ nm. The overlayer NCs on top of the hexagonal template follow the hexagonal symmetry of the underlying 2D hexagonal NC superlattice monolayer²⁹ to form a $[110]_{\text{SL}}$ -oriented bct superlattice (Figure 2a). The extracted nearest-neighbor interparticle (N–N) distance of the overlayer assembly (9.25 nm) on top of the hexagonal template is close to the N–N distance of the template (8.5 nm). The small difference in N–N distance is attributed to the compressive strain acting on the NCs by the existing lattice mismatch ($f_1 = 7.7\%$) of the template superlattice.

On the other hand, we observe fcc superlattice formation by the overlayer NCs on the surface of a square periodic superlattice (Figure 3a), where the in-plane overlayer NCs are arranged hexagonally at the interface. The extracted N–N distance (10.2 nm) is significantly larger than the N–N distance (9.25 nm) of the overlayer assembly, formed by the similar SP NCs on top of the hexagonal template. Formation of different in-plane structural symmetry (template, square; overlayer, hexagonal at in-plane) at the interface can be attributed to the interfacial surface reconstruction between the square template and hexagonal overlayer superlattice layers.²⁹ It has been reported previously that in the large misfit range ($f_2 = -24.4\%$), the overlayer crystal lattice can adopt any nontrivial registry patterns because of very low or no tensile strain between the interfacial layers.²⁹

Upon ligand treatment, the overlayer bct superlattice on the hexagonal template transforms its orientational axis from $[110]_{\text{SL}}$ to $[002]_{\text{SL}}$ -direction with respect to the templates, keeping the space group symmetry ($Im\bar{3}m$) unaltered (see Figure 2b). On the other hand, the overlayer $[111]_{\text{SL}}$ -oriented fcc superlattice on the square periodic template transforms into the $[002]_{\text{SL}}$ -oriented bcc superlattice, with entirely different symmetry ($Fm\bar{3}m \rightarrow Im\bar{3}m$). This transformation is attributed to the reorganization of the NCs into a more favorable configuration by maximizing the small CuTAPc adligands at the template–superlattice interface.³⁷ The appearance of new molecules at the interface reduces the interaction energy³⁸ between the template and overlayer, whereas their presence inbetween the NCs increases the facet–facet interactions via cross-coupling.^{30,39} Therefore, it is possible to tune the structure, symmetry, preferential orientation, and interplanar distance of the overlayer superlattice on top of the NC template by adding new small, rigid cross-linking molecules.

Several groups have already found that PbS NC superlattices undergo a structural transformation from fcc to bcc states (via bct), depending on the solvent vapor conditions,⁴⁰ slow cosolvent evaporation,⁴¹ and/or growth conditions⁴² of the NCs through Bain distortion. Recently, Novák et al. have observed the formation of a bct superlattice of cuboctahedral PbS NCs on the surface of silicon substrates.³⁹ Here, we note an important difference, where depending on the lattice misfit and template periodicity, the overlayer NCs assemble into either a soft epitaxial bct or fcc superlattice on top of the NC templates and transform their structure and crystallographic orientation upon ligand treatment. SP NCs form $[110]_{\text{SL}}$ -oriented bct superlattice on the hexagonal template, whereas

similar SP NCs form a $[111]_{\text{SL}}$ -oriented fcc superlattice on a square template. After ligand treatment, both bct and fcc superlattices transform into the $[002]_{\text{SL}}$ -oriented bcc superlattice. This structural transformation can be connected to that of a Bain distortion⁴³ through lattice reconstruction, in which the c -axis of the unit cell contracts whereas the other two axes (a and b) expand, causing the fcc-to-bcc transition through bct as an intermediate phase.^{40,41} In our case, the fcc superlattice parameters $a = b = c = 14.7$ nm transform into the bcc superlattice with $a = b = c = 11.0$ nm and bct superlattice parameters $a = b = 10.7$ nm and $c = 9.27$ nm contract into another bcc superlattice of $a = b = c = 10.4$ nm. This overall structural transformation and/or change in axial orientation ($[111]_{\text{SL}}$ or $[110]_{\text{SL}} \rightarrow [002]_{\text{SL}}$ -direction) needs a collective rotation of the superlattice and a large contraction/expansion of the unit cell axis through Bain distortion.^{40,43} The addition of short (1.4 nm) rigid CuTAPc molecules triggers the overall rotation of the overlayer superstructure and regulates the lattice parameters by increasing or decreasing the ligand coverage between the NCs.^{44,45}

To investigate the alignment of the NCs within the superlattice, we analyze the diffraction peak intensities of the GIXD patterns along the q_y -direction (in-plane azimuthal angle (δ)), integrating over a small q_z -window (Δq_z), which is proportionate to the orientational order of the NCs. We determine the orientation of the NCs in the template layer and in the corresponding overlayer assemblies on the basis of relative peak intensities from different atomic planes in the GIXD profiles (see Figures 2c,d and 3c,d).^{26,41} For the hexagonal template (SP-CuTAPc), a sharp intense 111_{NC} Bragg peak and a 200_{NC} peak of comparable intensity along the q_y -direction (Figure S2d) indicate the possibility of having an almost equal number of scatters, oriented with their $\{111\}_{\text{NC}}$ and $\{200\}_{\text{NC}}$ lattice planes, where NCs are arranged with their $\langle 111 \rangle$ and $\langle 200 \rangle$ facets pointing along the in-plane direction. For the overlayer of SP NCs on top of a hexagonal template, the appearance of intense diffraction peaks (with similar relative intensity ratio as template) from both the $\{111\}_{\text{NC}}$ and $\{200\}_{\text{NC}}$ lattice planes suggests no preferentially atomic arrangement of the NCs. This could be attributed to the stabilization of overlayer NCs by both types of preferential facet–facet ($\{200\}_{\text{NC}}-\{200\}_{\text{NC}}$ and $\{111\}_{\text{NC}}-\{111\}_{\text{NC}}$) interactions between the overlayer and template layer. Interestingly, upon ligand addition into that overlayer assembly, the NCs possess preferential atomic scattering from the $\{200\}_{\text{NC}}$ lattice plane where the $\langle 200 \rangle$ facet direction points upward. This is attributed to a strong in-plane directional interaction between $\{200\}_{\text{NC}}-\{200\}_{\text{NC}}$ atomic facets of the NCs via the cross-linker molecules,^{30,46} which is more dominant over the interfacial interaction between the overlayer and hexagonal template.

For a square template (CP-CuTAPc), we investigate that the cubic NCs show a strong in-plane diffraction peak from the $\{200\}_{\text{NC}}$ lattice planes, which implies that the NCs orient with their $\langle 200 \rangle$ facet pointing upward.^{30,33} The appearance of a strong diffraction peak from the $\{200\}_{\text{NC}}$ lattice planes from the SP NC overlayers on top of this template indicates that the atomic planes of the NCs have a tendency to orient with the $\{200\}_{\text{NC}}$ direction parallel to the templates, which is contrary to the overlayer assembly of similar NCs on top of the hexagonal template. This is attributed to the preferential interaction to the $\{200\}_{\text{NC}}$ facets of SP NCs by the oriented $\{200\}_{\text{NC}}-\text{CP}$ NC facets pointing upward in the template. Here,

during the self-assembly, the NCs possibly get sufficient time to align preferentially via $\{200\}_{\text{NC}}-\{200\}_{\text{NC}}$ interaction as the existing CP NCs in the template are oriented with their $\langle 200 \rangle$ facets along upward direction. Upon ligand treatment in the overlayer assembly, the atomic orientation of the NCs does not change at all, although there is a complete change in the superlattice structure and orientation. This is attributed to the existing interfacial interaction between the $\{200\}_{\text{NC}}$ facets and the induced cross-linking by the new ligands. It is also important to note that for the ligand-treated overlayer assemblies, the $[002]_{\text{SL}}$ superlattice direction and $[200]_{\text{NC}}$ atomic lattice direction are parallel to each other, which implies the overlayer NCs form iso-oriented mesocrystal superlattices on top of differently designed NC templates. Therefore, this method has the potential to prepare highly oriented multilayers of coherent NC assemblies.

In conclusion, the soft epitaxial assembly of two nanocrystal superlattices into a coherent overlayer with structural registry is possible if the lattice mismatch does not significantly exceed 7.7%. Up to around this mismatch, different nanocrystal diameters and even surface ligands of different lengths or structural rigidity are tolerated. The structure and crystallographic orientation of the second superlattice layer can thus be controlled by virtue of the structure of the first superlattice as well as the choice of surface ligand. For a substantially higher lattice mismatch of 24.4%, as given in our example, strain between the two layers is released by the adoption of a different structure or orientation of the second superlattice to reduce the mismatch. These results provide important clues for the preparation of soft epitaxial, heterostructured nanocrystal multilayers with uniform superlattice structure and orientation.

■ ASSOCIATED CONTENT

Supporting Information

The Supporting Information is available free of charge on the ACS Publications website at DOI: 10.1021/acs.jpcl.9b02373.

Characterization of SP-CuTAPc template, experimental procedures, and supporting tables and figures (PDF)

■ AUTHOR INFORMATION

Corresponding Author

*E-mail: santanu.maiti@uni-tuebingen.de.

ORCID

Santanu Maiti: 0000-0003-1491-6688

Martin Hodas: 0000-0001-6328-1717

Marcus Scheele: 0000-0002-2704-3591

Frank Schreiber: 0000-0003-3659-6718

Notes

The authors declare no competing financial interest.

■ ACKNOWLEDGMENTS

This work was supported by the DFG under grants SCHE1905/3, SCHE1905/4, and SCHR700/25. We thank the European Synchrotron Radiation Facility (ESRF), Grenoble, France for enabling X-ray scattering experiments at beamline ID03. We thank Mrs. Nadler for SEM measurements. M.H. acknowledges the Alexander von Humboldt foundation for financial support.

■ REFERENCES

- (1) Barth, J. V.; Costantini, G.; Kern, K. Engineering atomic and molecular nanostructures at surfaces. *Nature* **2005**, *437*, 671–679.
- (2) Venables, J. A. Nucleation and Growth of Thin-Films - Recent Progress. *Vacuum* **1983**, *33*, 701–705.
- (3) Zhang, Z. Y.; Lagally, M. G. Atomistic processes in the early stages of thin-film growth. *Science* **1997**, *276*, 377–383.
- (4) Storhoff, J. J.; Lazarides, A. A.; Mucic, R. C.; Mirkin, C. A.; Letsinger, R. L.; Schatz, G. C. What controls the optical properties of DNA-linked gold nanoparticle assemblies? *J. Am. Chem. Soc.* **2000**, *122*, 4640–4650.
- (5) Sargent, E. H. Colloidal quantum dot solar cells. *Nat. Photonics* **2012**, *6*, 133–135.
- (6) Evanoff, D. D.; Chumanov, G. Synthesis and optical properties of silver nanoparticles and arrays. *ChemPhysChem* **2005**, *6*, 1221–1231.
- (7) Choi, J. H.; Wang, H.; Oh, S. J.; Paik, T.; Jo, P. S.; Sung, J.; Ye, X. C.; Zhao, T. S.; Diroll, B. T.; Murray, C. B.; Kagan, C. R. Exploiting the colloidal nanocrystal library to construct electronic devices. *Science* **2016**, *352*, 205–208.
- (8) Shevchenko, E. V.; Talapin, D. V.; Kotov, N. A.; O'Brien, S.; Murray, C. B. Structural diversity in binary nanoparticle superlattices. *Nature* **2006**, *439*, 55–59.
- (9) Milliron, D. J.; Hughes, S. M.; Cui, Y.; Manna, L.; Li, J. B.; Wang, L. W.; Alivisatos, A. P. Colloidal nanocrystal heterostructures with linear and branched topology. *Nature* **2004**, *430*, 190–195.
- (10) Maiti, S.; Sanyal, M. K.; Varghese, N.; Satpati, B.; Dasgupta, D.; Daillant, J.; Carriere, D.; Konovolov, O.; Rao, C. N. R. Formation of single-crystalline CuS at the organic-aqueous interface. *J. Phys.: Condens. Matter* **2013**, *25*, No. 395401.
- (11) Belman, N.; Acharya, S.; Konovolov, O.; Vorobiev, A.; Israelachvili, J.; Efrima, S.; Golan, Y. Hierarchical Assembly of Ultrathin Alkylamine-Coated ZnS Nanorods: A Synchrotron Surface X-Ray Diffraction Study. *Nano Lett.* **2008**, *8*, 3858–3864.
- (12) Tao, A.; Kim, F.; Hess, C.; Goldberger, J.; He, R. R.; Sun, Y. G.; Xia, Y. N.; Yang, P. D. Langmuir-Blodgett silver nanowire monolayers for molecular sensing using surface-enhanced Raman spectroscopy. *Nano Lett.* **2003**, *3*, 1229–1233.
- (13) Hellstrom, S. L.; Kim, Y.; Fakonas, J. S.; Senesi, A. J.; Macfarlane, R. J.; Mirkin, C. A.; Atwater, H. A. Epitaxial Growth of DNA-Assembled Nanoparticle Superlattices on Patterned Substrates. *Nano Lett.* **2013**, *13*, 6084–6090.
- (14) Whitham, K.; Yang, J.; Savitzky, B. H.; Kourkoutis, L. F.; Wise, F.; Hanrath, T. Charge transport and localization in atomically coherent quantum dot solids. *Nat. Mater.* **2016**, *15*, 557–563.
- (15) Zhao, T. S.; Goodwin, E. D.; Guo, J.; Wang, H.; Diroll, B. T.; Murray, C. B.; Kagan, C. R. Advanced Architecture for Colloidal PbS Quantum Dot Solar Cells Exploiting a CdSe Quantum Dot Buffer Layer. *ACS Nano* **2016**, *10*, 9267–9273.
- (16) Zaluzhnyy, I. A.; Kurta, R. P.; André, A.; Gorobtsov, O. Y.; Rose, M.; Skopintsev, P.; Besedin, I.; Zozulya, A. V.; Sprung, M.; Schreiber, F.; Vartanyants, I. A.; Scheele, M. Quantifying Angular Correlations between the Atomic Lattice and the Superlattice of Nanocrystals Assembled with Directional Linking. *Nano Lett.* **2017**, *17*, 3511–3517.
- (17) Weidman, M. C.; Nguyen, Q.; Smilgies, D. M.; Tisdale, W. A. Impact of Size Dispersity, Ligand Coverage, and Ligand Length on the Structure of PbS Nanocrystal Superlattices. *Chem. Mater.* **2018**, *30*, 807–816.
- (18) Walravens, W.; De Roo, J.; Drijvers, E.; ten Brinck, S.; Solano, E.; Dendooven, J.; Detavernier, C.; Infante, I.; Hens, Z. Chemically Triggered Formation of Two-Dimensional Epitaxial Quantum Dot Superlattices. *ACS Nano* **2016**, *10*, 6861–6870.
- (19) Evers, W. H.; Goris, B.; Bals, S.; Casavola, M.; de Graaf, J.; van Roij, R.; Dijkstra, M.; Vanmaekelbergh, D. Low-Dimensional Semiconductor Superlattices Formed by Geometric Control over Nanocrystal Attachment. *Nano Lett.* **2013**, *13*, 2317–2323.
- (20) Savitzky, B. H.; Hovden, R.; Whitham, K.; Yang, J.; Wise, F.; Hanrath, T.; Kourkoutis, L. F. Propagation of Structural Disorder in

Epitaxially Connected Quantum Dot Solids from Atomic to Micron Scale. *Nano Lett.* **2016**, *16*, 5714–5718.

(21) Schliehe, C.; Juarez, B. H.; Pelletier, M.; Jander, S.; Greshnykh, D.; Nagel, M.; Meyer, A.; Foerster, S.; Kornowski, A.; Klinke, C.; Weller, H. Ultrathin PbS Sheets by Two-Dimensional Oriented Attachment. *Science* **2010**, *329*, 550–553.

(22) Whitham, K.; Hanrath, T. Formation of Epitaxially Connected Quantum Dot Solids: Nucleation and Coherent Phase Transition. *J. Phys. Chem. Lett.* **2017**, *8*, 2623–2628.

(23) Boneschanscher, M. P.; Evers, W. H.; Geuchies, J. J.; Altantzis, T.; Goris, B.; Rabouw, F. T.; van Rossum, S. A. P.; van der Zant, H. S. J.; Siebbeles, L. D. A.; Van Tendeloo, G.; Swart, I.; Hilhorst, J.; Petukhov, A. V.; Bals, S.; Vanmaekelbergh, D. Long-range orientation and atomic attachment of nanocrystals in 2D honeycomb superlattices. *Science* **2014**, *344*, 1377–1380.

(24) Maiti, S.; Sanyal, M. K.; Jana, M. K.; Runge, B.; Murphy, B. M.; Biswas, K.; Rao, C. N. R. Evidence of contact epitaxy in the self-assembly of HgSe nanocrystals formed at a liquid-liquid interface. *J. Phys.: Condens. Matter* **2017**, *29*, No. 095101.

(25) van der Stam, W.; Rabouw, F. T.; Vonk, S. J. W.; Geuchies, J. J.; Ligthart, H.; Petukhov, A. V.; Donega, C. D. Oleic Acid-Induced Atomic Alignment of ZnS Polyhedral Nanocrystals. *Nano Lett.* **2016**, *16*, 2608–2614.

(26) Geuchies, J. J.; van Overbeek, C.; Evers, W. H.; Goris, B.; de Backer, A.; Gantapara, A. P.; Rabouw, F. T.; Hilhorst, J.; Peters, J. L.; Konovalov, O.; Petukhov, A. V.; Dijkstra, M.; Siebbeles, L. D. A.; van Aert, S.; Bals, S.; Vanmaekelbergh, D. In situ study of the formation mechanism of two-dimensional superlattices from PbSe nanocrystals. *Nat. Mater.* **2016**, *15*, 1248–1254.

(27) Wang, Z. W.; Schliehe, C.; Bian, K. F.; Dale, D.; Bassett, W. A.; Hanrath, T.; Klinke, C.; Weller, H. Correlating Superlattice Polymorphs to Internanoparticle Distance, Packing Density, and Surface Lattice in Assemblies of PbS Nanoparticles. *Nano Lett.* **2013**, *13*, 1303–1311.

(28) Wang, M. X.; Seo, S. E.; Gabrys, P. A.; Fleischman, D.; Lee, B.; Kim, Y.; Atwater, H. A.; Macfarlane, R. J.; Mirkin, C. A. Epitaxy: Programmable Atom Equivalents Versus Atoms. *ACS Nano* **2017**, *11*, 180–185.

(29) Rupich, S. M.; Castro, F. C.; Irvine, W. T. M.; Talapin, D. V. Soft epitaxy of nanocrystal superlattices. *Nat. Commun.* **2014**, *5*, 5045.

(30) Maiti, S.; Maiti, S.; Maier, A.; Hagenlocher, J.; Chumakov, A.; Schreiber, F.; Scheele, M. Understanding the Formation of Conductive Mesocrystalline Superlattices with Cubic PbS Nanocrystals at the Liquid/Air Interface. *J. Phys. Chem. C* **2019**, *123*, 1519–1526.

(31) Maiti, S.; André, A.; Banerjee, R.; Hagenlocher, J.; Konovalov, O.; Schreiber, F.; Scheele, M. Monitoring Self-Assembly and Ligand Exchange of PbS Nanocrystal Superlattices at the Liquid/Air Interface in Real Time. *J. Phys. Chem. Lett.* **2018**, *9*, 739–744.

(32) Scheele, M.; Brütting, W.; Schreiber, F. Coupled organic-inorganic nanostructures (COIN). *Phys. Chem. Chem. Phys.* **2015**, *17*, 97–111.

(33) André, A.; Theurer, C.; Lauth, J.; Maiti, S.; Hodas, M.; Samadi Khoshkhoo, M.; Kinge, S.; Meixner, A. J.; Schreiber, F.; Siebbeles, L. D.; Braun, K.; Scheele, M. Structure, transport and photoconductance of PbS quantum dot monolayers functionalized with a copper phthalocyanine derivative. *Chem. Commun.* **2017**, *53*, 1700–1703.

(34) Tate, M. P.; Hillhouse, H. W. General method for simulation of 2D GISAXS intensities for any nanostructured film using discrete Fourier transforms. *J. Phys. Chem. C* **2007**, *111*, 7645–7654.

(35) Renaud, G.; Lazzari, R.; Leroy, F. Probing surface and interface morphology with Grazing Incidence Small Angle X-Ray Scattering. *Surf. Sci. Rep.* **2009**, *64*, 255–380.

(36) Jiang, Z. GIXSGUI: a MATLAB toolbox for grazing-incidence X-ray scattering data visualization and reduction, and indexing of buried three-dimensional periodic nanostructured films. *J. Appl. Crystallogr.* **2015**, *48*, 917–926.

(37) Senesi, A. J.; Eichelsdoerfer, D. J.; Macfarlane, R. J.; Jones, M. R.; Auyeung, E.; Lee, B.; Mirkin, C. A. Stepwise Evolution of DNA-

Programmable Nanoparticle Superlattices. *Angew. Chem., Int. Ed.* **2013**, *52*, 6624–6628.

(38) Bian, K. F.; Choi, J. J.; Kaushik, A.; Clancy, P.; Smilgies, D. M.; Hanrath, T. Shape-Anisotropy Driven Symmetry Transformations in Nanocrystal Superlattice Polymorphs. *ACS Nano* **2011**, *5*, 2815–2823.

(39) Novak, J.; Banerjee, R.; Kornowski, A.; Jankowski, M.; André, A.; Weller, H.; Schreiber, F.; Scheele, M. Site-Specific Ligand Interactions Favor the Tetragonal Distortion of PbS Nanocrystal Superlattices. *ACS Appl. Mater. Interfaces* **2016**, *8*, 22526–22533.

(40) Bian, K. F.; Wang, Z. W.; Hanrath, T. Comparing the Structural Stability of PbS Nanocrystals Assembled in fcc and bcc Superlattice Allotropes. *J. Am. Chem. Soc.* **2012**, *134*, 10787–10790.

(41) Weidman, M. C.; Smilgies, D. M.; Tisdale, W. A. Kinetics of the self-assembly of nanocrystal superlattices measured by real-time in situ X-ray scattering. *Nat. Mater.* **2016**, *15*, 775–781.

(42) Bian, K. F.; Li, R. P.; Fan, H. Y. Controlled Self-Assembly and Tuning of Large PbS Nanoparticle Supercrystals. *Chem. Mater.* **2018**, *30*, 6788–6793.

(43) Singh, S.; Dutta, B.; D'Souza, S. W.; Zavareh, M. G.; Devi, P.; Gibbs, A. S.; Hickel, T.; Chadov, S.; Felser, C.; Pandey, D. Robust Bain distortion in the premartensite phase of a platinum-substituted Ni₂MnGa magnetic shape memory alloy. *Nat. Commun.* **2017**, *8*, 1006.

(44) Bian, K. F.; Schunk, H.; Ye, D. M.; Hwang, A.; Luk, T. S.; Li, R. P.; Wang, Z. W.; Fan, H. Y. Formation of self-assembled gold nanoparticle supercrystals with facet-dependent surface plasmonic coupling. *Nat. Commun.* **2018**, *9*, 2365.

(45) Goodfellow, B. W.; Yu, Y. X.; Bosoy, C. A.; Smilgies, D. M.; Korgel, B. A. The Role of Ligand Packing Frustration in Body-Centered Cubic (bcc) Superlattices of Colloidal Nanocrystals. *J. Phys. Chem. Lett.* **2015**, *6*, 2406–2412.

(46) Choi, J. J.; Bealing, C. R.; Bian, K. F.; Hughes, K. J.; Zhang, W. Y.; Smilgies, D. M.; Hennig, R. G.; Engstrom, J. R.; Hanrath, T. Controlling Nanocrystal Superlattice Symmetry and Shape-Anisotropic Interactions through Variable Ligand Surface Coverage. *J. Am. Chem. Soc.* **2011**, *133*, 3131–3138.